Journal of
Composites Science

MDPI

Article

Effects of Topological Parameters on Thermal Properties of Carbon Nanotubes via Molecular Dynamics Simulation

Lida Najmi and Zhong Hu *

Department of Mechanical Engineering, J.J. Lohr College of Engineering/Brookings, South Dakota State University, Brookings, SD 57007, USA; lida.najmi@jacks.sdstate.edu
* Correspondence: zhong.hu@sdstate.edu; Tel.: +1-605-688-4817

Abstract: Due to their unique properties, carbon nanotubes (CNTs) are finding a growing number of applications across multiple industrial sectors. These properties of CNTs are subject to influence by numerous factors, including the specific chiral structure, length, type of CNTs used, diameter, and temperature. In this topic, the effects of chirality, diameter, and length of single-walled carbon nanotubes (SWNTs) on the thermal properties were studied using the reverse non-equilibrium molecular dynamics (RNEMD) method and the Tersoff interatomic potential of carbon–carbon based on the Large-scale Atomic/Molecular Massively Parallel Simulator (LAMMPS). For the shorter SWNTs, the effect of chirality on the thermal conductivity is more obvious than for longer SWNTs. Thermal conductivity increases with increasing chiral angle, and armchair SWNTs have higher thermal conductivity than that of zigzag SWNTs. As the tube length becomes longer, the thermal conductivity increases while the effect of chirality on the thermal conductivity decreases. Furthermore, for SWNTs with longer lengths, the thermal conductivity of zigzag SWNTs is higher than that of the armchair SWNTs. Thermal resistance at the nanotube–nanotube interfaces, particularly the effect of CNT overlap length on thermal resistance, was studied. The simulation results were compared with and in agreement with the experimental and simulation results from the literature. The presented approach could be applied to investigate the properties of other advanced materials.

Keywords: carbon nanotubes (CNTs); single-walled carbon nanotubes (SWNTs); chirality; aspect ratio; topological parameter; thermal properties; molecular dynamics (MD) simulations

check for updates

Citation: Najmi, L.; Hu, Z. Effects of Topological Parameters on Thermal Properties of Carbon Nanotubes via Molecular Dynamics Simulation. *J. Compos. Sci.* **2024**, *8*, 37. https://doi.org/10.3390/jcs8010037

Academic Editor: Francesco Tornabene

Received: 14 December 2023
Revised: 16 January 2024
Accepted: 19 January 2024
Published: 22 January 2024

1. Introduction

The demand for polymeric composites has grown significantly due to the requirements of human communities and industries for the construction of lightweight, strong, and durable structures, as well as the need for highly conductive materials [1–3]. Among the various options for the reinforcement of polymeric matrix nanocomposites, carbon-based nanofillers, including carbon nanotubes (CNTs) and graphene nanoplatelets (GNPs), could help to achieve the desired improvement in the thermal conductivity of the nanocomposites [4–6]. CNTs have special properties such as high strength, lightweight, unique electronic structure, and high stability, making them ideal materials for a wide range of applications. The thermal conductivity of nanomaterials plays a crucial role in controlling the performance and stability of nanocomposites in nano/micro-devices [7–9]. CNTs can be categorized into three main types based on their number of layers: single-walled CNTs (SWNTs), double-walled CNTs (DWNTs), and multi-walled CNTs (MWNTs) [10–16].

The conductive properties of CNTs, depending on their structures (individual, films, bundled, buckypaper, etc.) and synthesis methods, demonstrate different values of thermal conductivity, from the level of thermal insulation with the thermal conductivity of 0.1 W/m·K for MWNTs to such high values as 6600 W/m·K for SWNTs. Berber et al. conducted MD simulations using the Tersoff potential to calculate the thermal conductivity of isolated (10, 10) CNTs and obtained an unusually high value of thermal conductivity of

6600 W/m·K at room temperature. Those high values of thermal conductivity are associated with the large-phonon mean free paths in their systems, which result from the long length of CNTs and high number of atoms in each unit cell. This result is comparable to the thermal conductivity of a hypothetical isolated graphene monolayer [17,18].

Che et al. focused on the theoretical consideration of the effect of vacancy or defect concentration on the thermal conductivity of CNTs. The theoretical value of an ideal SWNT measured along the tube axis is approximately 2980 W/m·K. Simulations of SWNTs with different defect or vacancy concentrations show that, as expected, the thermal conductivity decreases with increasing defect or vacancy concentration. Additionally, it was discovered that the thermal conductivity changes when the CNTs are not individual CNTs but bundled together in a closely packed condition. The thermal conductivity along the axis is 950 W/m·K, but the thermal conductivity in the perpendicular direction is only 5.6 W/m·K. This indicates that the thermal conductivity of CNTs is much lower in the transverse direction than in the longitudinal direction. These extreme differences in thermal conductivity indicate that MWNTs and CNT bundles and ropes exhibit varying degrees of thermal conductivity [19].

There are two main principles on how to hinder efficient transportation. First, despite using the most precise reaction control systems, CNTs always have inherent flaws. Topological defects such as the Stone–Wales-type topological defects or simple vacancies can cause scattering, thereby reducing the mean free path of phonons. Second, CNTs always contain some form of extraneous contaminants (other forms of carbon, residual catalyst, etc.) that must be removed so as not to interfere with high-performance thermal energy transfer. The decrease in thermal conductivity of SWNTs was reported by Park et al. and Chien et al. using reverse non-equilibrium molecular dynamics (RNEMD) simulations [20,21]. Park et al.'s research shows that the concentration of vacancy defect (up to 2%) can reduce thermal conductivity by more than 80%. It must also be noted that Park's research focused on (6, 6) SWNTs of varying lengths as opposed to (10, 10) SWNTs in the study conducted by Chien et al. The results show that the introduction of vacancies reduces the thermal conductivity to about 0.5 W/m·K. The main reason for the decrease in thermal conductivity is that the lack of bonds around the vacancies immediately terminates short-wavelength phonons.

Another important factor affecting the thermal conductivity of MWNTs is the interlayer distance of MWNTs. Smaller interlayer distances can enhance van der Waals interactions between adjacent layers. This affects phonon scattering and thermal transport along the nanotube axis. Variations in interlayer distance may also introduce defects or disorder, which in some cases can reduce thermal conductivity as low as 0.1 W/m·K [22,23].

Alaghemandi et al. used RNEMD simulations and showed that changes in the bond length of carbon atoms have very little effect on the thermal conductivity of SWNTs. They showed that reducing the bond length (Δr = 0.12 Å) of (10, 10) nanotubes with a diameter of D = 1.40 nm and length of L = 96.1 nm can increase the thermal conductivity by approximately 3% [24].

SWNTs can form three different designs: armchair, chiral, and zigzag. Armchair CNTs have electrical properties similar to metals, but the other two structures have electrical properties similar to semiconductors [25,26]. The use of CNTs with a higher aspect ratio (length/diameter) is an efficient means to obtain better thermal conductivity enhancement in CNT-modified polymer composites. Thus, as the tube length increases, the thermal conductivity increases, while the effect of chirality on the thermal conductivity decreases [27].

Since there are many factors affecting the performance of CNT-modified composites and some of which affect material performance at the nanoscale, conventional experimental techniques and continuum modeling methods cannot characterize them. Traditional trial-and-error experimental approaches are expensive, time-consuming, and sometimes impossible [28]. Therefore, an effective design is needed to develop novel composites with desired properties for applications. Molecular dynamics (MD) or first-principles simulations are excellent tools for studying material properties at the nanoscale. In the classical MD method, electronic effects are averaged, and the simulation focuses on calculating the

time evolution of atomic positions and velocities in accordance with Newton's equations of motion.

The interatomic potentials (force fields) are developed from the first principles or derived from experimental data to describe the interactions between atoms. The reliability of these interatomic potentials plays a crucial role in determining the precision of MD simulations and their capacity to bridge the effectiveness of mesoscale methods [29–32]. One of the most notable interatomic potentials is the Lennard–Jones potential. It has long been used to describe rare gas atoms, simple metals, and highly ionic systems. On the other hand, many-body potentials, including additional terms for many-body interactions, have been proposed and applied to materials such as semiconductors and polymers [33,34]. Tersoff potential is one of the best-known potentials and provides a realistic description of the bond order in terms of the local environment (number of neighbors). The Tersoff potential is generally designed to model materials with covalent bonding and is often applied to systems where atoms have a preferred coordination number, such as quadruple coordination in diamond or silicon carbide [35].

Many studies have been carried out on the relationship between the thermal conductivity of CNTs and other influential factors such as length, temperature, and diameter of CNTs to find the optimum conditions for industrial applications. Osman and Srivastava [36] and Cao et al. [37] studied the effect of temperature on the thermal conductivity of SWNTs. The results show that as the temperature increases, the thermal conductivity first increases and then decreases, but there is no consensus on the cause of temperature peak. Varshney et al. [38] and Hou et al. [39] studied the effect of length on the thermal conductivity of CNTs, and the results show that the thermal conductivity increased with the increase in length. For the effect of diameter, Varshney et al. [38] and Li et al. [40] proposed that the effect of diameter on the thermal conductivity of CNTs may be different for CNTs with different lengths. Chirality is a distinctive feature of SWNTs, and it is known that the chiral angle plays a crucial role in determining various physical properties, including thermal conductivity. Surprisingly, its effect on the thermal conductivity of SWNTs remains unclear. Zhang et al. [41] determined, based on their calculations, that zigzag SWNTs have a higher thermal conductivity than armchair SWNTs. There are limited studies examining the relationship between chirality and thermal conductivity. Experimental attempts to quantify the heat transfer properties of SWNTs have encountered many difficulties, and MD simulations have proven to be of great help in the ongoing catalog of CNT heat transfer properties. However, Hone et al. [42] showed that experimental measurements of SWNT samples revealed a room temperature conductivity of approximately 35 W/m·K. Lukes and Zhong [43] also investigated the thermal conductivity of individual (10, 10) SWNTs using MS simulations as a function of length, temperature, boundary conditions, and MS simulation methodology. Their results indicate that thermal conductivity increases with nanotube length, varying from about 10 W/mK to 375 W/mK.

Thermal resistance (R) can be a significant obstacle to heat transfer through polymer nanocomposites [44]. Since the heat transfer in these composites is primarily governed by phonon transfer, the interfacial thermal resistance is attributed to the phonon scattering at the filler–matrix and filler–filler interfaces [45], which hinders the heat flux through the composites, thus reducing its effective thermal conductivity. Different factors affect the magnitude of R, but the most important factor is the length of interface overlap. The most challenging part is to develop an accurate molecular model of the interfacial segments, which can then be used to evaluate R in different geometrical configurations [46].

Therefore, this study will investigate the effects of topological parameters of SWNTs, including chiral angle, length, diameter, and other parameters on the thermal properties of SWNTs based on the Tersoff potential using RNEMD simulations. The effect of nanotube–nanotube overlapping length on thermal resistance (R_{CC}) will also be investigated. The simulation results will be compared with the experimental and computer modeling results from the literature for validation.

2. Molecular Dynamics Simulation Methodology

2.1. RNEMD Approach

Reverse non-equilibrium molecular dynamics (RNEMD) based on the Müller-Plathe's approach was used to calculate the thermal conductivity of CNTs. RNEMD reverses the usual cause and effect picture. In this approach, the simulation box is divided into 5 bins along the *z*-axis. Both end regions are designated as the lower-temperature zone, while the middle bin is the higher-temperature zone (as shown in Figure 1). The heat flux is then imposed on the system as a primary perturbation. In the RNEMD method, the thermal energy is continuously interchanged, in an artificial manner, between the 'cold' region and the 'hot' region by exchanging the velocity of the hottest atom (v_{hot}) in the cold region with the velocity of the coldest atoms (v_{cold}) in the hot region, and then the temperature gradient is obtained from the simulation. This makes the simulations converge faster relative to the non-equilibrium MD method, in which a thermal gradient is applied, and the heat flux is measured instead. In fact, the simulated heat flux typically exhibits large fluctuations and therefore converges slowly. However, thermal gradients averaged over time and space tend to converge in a faster manner. By repeating the transfer at regular intervals, an artificial heat flux j_z is generated and calculated as [47]:

$$j_z = \frac{1}{2tA} \sum \frac{m}{2} \left(v_{hot}^2 - v_{cold}^2 \right) \tag{1}$$

where m is the atomic mass, t is the simulation time, and A is the cross-sectional area of the simulation box. v_{hot} and v_{cold} are the velocities of the selected atoms in the hot region and cold region, respectively. When a steady state is reached, the amount of energy per time and area (this is the definition of the heat flux j_z) flowing from the hot to the cold region via heat conduction can be obtained. Consequently, j_z induces a temperature gradient $\langle \partial T/\partial z \rangle$ across the system, from which the thermal conductivity, λ, can be determined using Fourier's law [48]:

$$\lambda = \lim_{\partial T/\partial z \to 0} \lim_{t \to \infty} -\frac{(j_z(t))}{(\partial T/\partial z)} \tag{2}$$

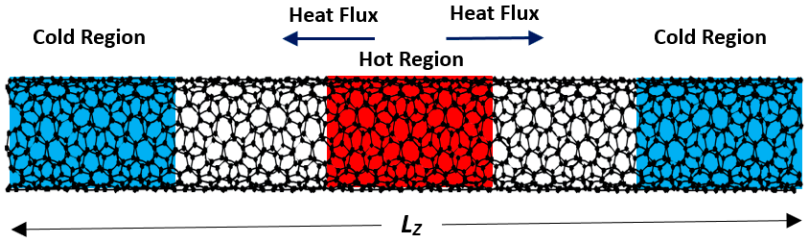

Figure 1. Reverse non-equilibrium molecular dynamics (RNEMD) approach employed to compute the thermal conductivity of SWNTs.

After the simulation is completed, results for temperature, z-direction coordination, and heat flux of the simulation box were obtained for each time step. The thermal conductivity of CNTs can be calculated using Microsoft Office 365 Excel or MATLAB 2023b to substitute the obtained results into Equation (2).

The RNEMD method can also be employed to calculate the thermal resistance, R, at the CNT–CNT interfaces. Under steady-state conditions, the calculated R under certain temperature drop (ΔT) and heat flux (j_z) across the CNT–CNT interface can be determined as [49]:

$$R = \frac{\Delta T}{j_z} \tag{3}$$

The adopted interatomic potential function affects the thermal conductivity calculation of CNTs. Salaway and Zhigilei [50] showed that CNTs with a Tersoff interatomic potential have higher and more accurate simulated thermal conductivity than those by Brenner-II

and AIREBO potentials, respectively. This is the main reason why Tersoff interatomic potential is used in this study. The electrostatic term is considered in the potential. It is combined into the potential function and does not have a separate term. If a chemical reaction in a reactive MD simulation is involved, the potential function will have a separate term to represent the relationship between the reacting atoms. Some key features of the Tersoff potential include three-body interaction, angular dependence, material-specific parameters, and computational efficiency [35].

2.2. Chiral Angle

Figure 2 is a schematic diagram of the chirality of a graphene sheet or an expanded CNT, in which the vector $\boldsymbol{S} = m\,\boldsymbol{a}_1 + n\,\boldsymbol{a}_2$ represents the chirality and diameter of SWNTs. Here, $\boldsymbol{a}_1$ and $\boldsymbol{a}_2$ symbolize the unit vectors of the graphene for constructing chiral angles. Furthermore, $\boldsymbol{S}$ denotes the lattice vector of two-dimensional graphene, while m and n are integers. The diameter of an SWNT is defined accordingly as:

$$d = \frac{|\boldsymbol{S}|}{\pi} = a\frac{\sqrt{m^2 + mn + n^2}}{\pi} \tag{4}$$

where $a = 1.42\sqrt{3}$ (nm) is the lattice constant. An armchair SWNT is defined when $m = n$. Conversely, a zigzag SWNT is determined when $m = 0$ or $n = 0$. Chirality encompasses crossing angles that span from zigzag SWNTs to armchair SWNTs, with a crossing angle of 30° in between. As a result, the chiral angle is the angle between the vector $\boldsymbol{S}$ and the orientation of the zigzag SWNT [25,27,51]. It is represented as

$$\theta = \tan^{-1}\left|\sqrt{3}n/(2m + n)\right| \tag{5}$$

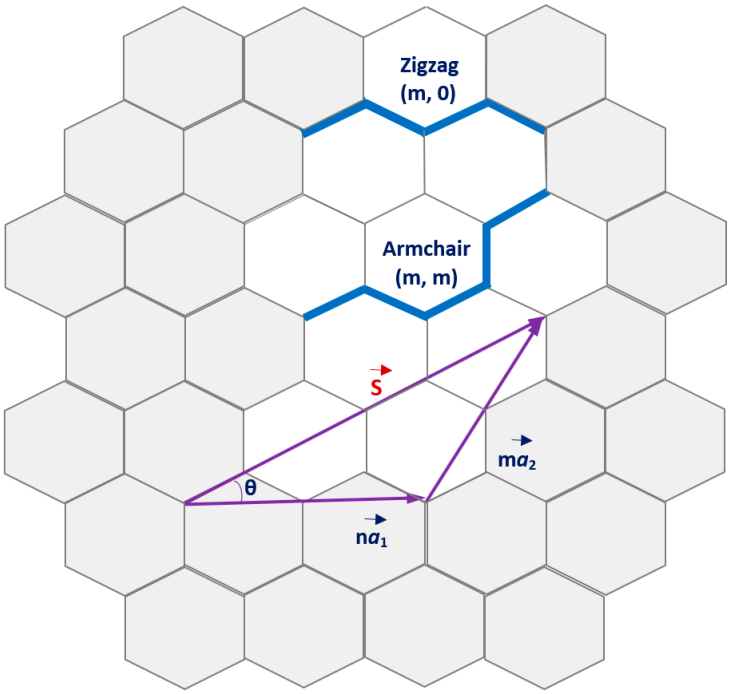

Figure 2. Schematic diagram of the chirality of a graphene hexagonal lattice with lattice vectors $\boldsymbol{a}_1$ and $\boldsymbol{a}_2$.

All the presented simulations were performed using the Large-scale Atomic/Molecular Massively Parallel Simulator (LAMMPS), an open resource MD simulation package, and Tersoff [52] force fields have been used for CNTs. After careful evaluation of the equilibrium state achieved for the simulation system during the simulation process under the given conditions, unless otherwise stated, all the setups were initially energy-minimized and

subsequently equilibrated in a canonical ensemble at 300 K for up to 300 ps (duration depended on the system size) using a time step of 0.5 fs (determined after simulation convergence study on time step). After equilibration, the thermal properties were calculated using the RNEMD method. To ensure accurate statistical results, the production run time was extended to 2 ns, allowing the simulated systems to achieve stable temperature and heat flux.

The systems studied here were constructed by repeating the unit cell of zigzag, chiral, and armchair nanotubes with different diameters and lengths. The simulation cells were elongated in the z-direction, which is also the direction of the energy flow; their lengths varied from 5 to 20 nm. The length parameter was smaller than typical experimental values due to the limitation of the simulation box size. Further computational details and simulation methods will be discussed in each specific subsection of the Results section.

Carbon–carbon bond behavior can be modeled in MD by employing the Tersoff interatomic potential. In 1988, Tersoff proposed the potential to simulate the behavior of the primary bonds between atoms in inorganic materials [52,53]. The cut-off distance for interatomic interactions in the Tersoff potential was chosen to be 1.95 Å to simulate C–C bonds.

3. Results and Discussion

3.1. Length Dependence of the Thermal Conductivity

The relationship between CNT length and thermal conductivity was studied using the RNEMD method, and the length dependence of the thermal conductivity λ of SWNTs with the same dimeter and different chiral indices of (5, 0) and (8, 8) at room temperature was studied. For each chiral model, the length parameter varied between 5 and 20 nm, with a diameter of approximately 0.65 nm. Referring to Figure 1, the heat flows from the hotter central region of the CNT to the colder regions located at the ends of the CNT. The results listed in Table 1 and shown in Figure 3 show that λ increases with L due to the presence of longer wavelength phonons. When the coefficient of determination $R^2 > 0.98$ a power-like trend is observed for both chiralities, i.e., [24,38,54,55]:

$$\lambda = A\, L^B \tag{6}$$

Table 1. The thermal conductivity λ changing with the length L of SWNTs.

SWNT Length *L* (nm)	**5**	**10**	**15**	**20**
λ (W/mK) of armchair (5, 5) (this research)	35.32	58.25	80.98	92.00
λ (W/mK) of zigzag (8, 0) (this research)	28.92	52.66	77.27	100.5
λ (W/mK) of armchair (10, 10) (from the literature)	40.40	60.00	78.5	90.00
λ (W/mK) of zigzag (10, 0) (from the literature)	32.56	55.68	80.00	105.0

The results showed that for (5, 5) zigzag SWNT, A = 11.95 and B = 0.7, and for (8, 8) zigzag SWNT, A = 7.14 and B = 0.89. The figure shows that the gap between the thermal conductivity λ curves is widest for shorter tube lengths and decreases with increases in length. This implies that the effect of chirality on thermal conductivity decreases for longer tubes, eventually resulting in a greater thermal conductivity for zigzag SWNTs with a length of 20 nm than for armchair SWNTs.

This is consistent with the length dependence found in other MD studies. Moreland et al. [56] showed that for length <100 nm, B = 0.78. Furthermore, Maruyama [57] showed that for chirality (5, 5) and length <400 nm, the exponent B is approximately 0.4. These results are consistent with the theoretical study at room temperature by Wang et al. [58]. For CNTs with a length <100 nm, the observed exponent B is 0.83. For CNTs with a length >10,000 nm, the observed exponent B is 0.35. The parameters of the power law (Equation (6)) can be obtained through data regression based on the data from Table 1 and Figure 3 and are listed in Table 2.

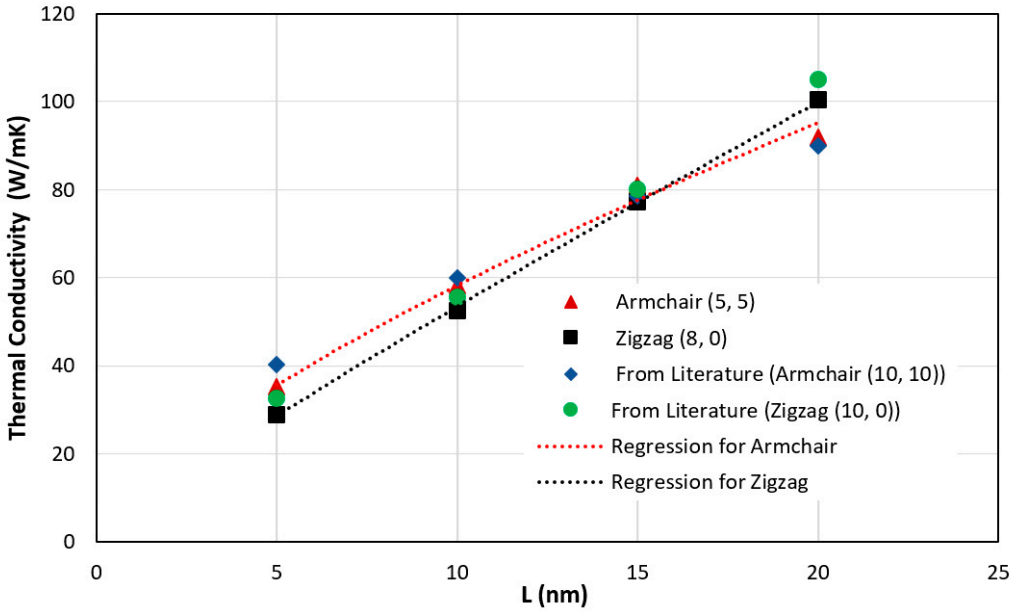

Figure 3. Thermal conductivity versus tube length of zigzag and armchair SWNTs with constant diameter (0.65 nm) at room temperature (300 K).

Table 2. The power law regression results based on the data from Table 1 and Figure 3.

MD Simulation Case	Regression Formula	R^2
λ (W/mK) of armchair (5, 5) (this research)	$\lambda = 11.397L^{0.7084}$	0.9892
λ (W/mK) of zigzag (8, 0) (this research)	$\lambda = 6.7471L^{0.8995}$	0.9997
λ (W/mK) of armchair (10, 10) (from the literature)	$\lambda = 15.706L^{0.5865}$	0.9972
λ (W/mK) of zigzag (10, 0) (from the literature)	$\lambda = 8.2714L^{0.8411}$	0.9976

In Figure 3, the lines for the armchair and zigzag SWNTs cross by around 16 nm. There may be multiple factors that affect the overall thermal conductivity of the chiral SWNTs. In the shorter SWNTs, if both armchair and zigzag SWNTs undergo similar scattering mechanisms and the impact on the overall thermal conductivity is smaller, and if the majority of phonons in both armchair and zigzag SWNTs propagate strictly along the theoretical pathways, the pathway length of the zigzag SWNTs is about 15.5% longer than that of the armchair SWNTs, and the thermal conductivity of an armchair SWNT will be 15.5% higher than that of a zigzag SWNT, which is consistent with the results for the shorter-tube-length SWNTs in Figure 3. In the longer SWNTs, phonons have more opportunities to propagate and scatter within the nanotubes. The overall thermal conductivity is affected by the ability of phonons to propagate along the tube and the scattering events that occur. Therefore, the longer SWNTs may have more phonon traveling modes than the shorter SWNTs, thereby reducing the effect of the chirality and inducing the crossing point at a certain tube length (around 16 nm in Figure 3). There are some other factors that may affect the phonon propagate pathways, scattering processes, and the overall thermal conductivity of the chiral SWNTs, such as SWNT lattice defects, interactions with the substrate and among the CNTs, or environmental conditions, which are not considered in this study.

3.2. Chiral Angle and Diameter Dependence of the Thermal Conductivity

In order to more objectively reflect the effect of chirality on thermal conductivity, the tube length and diameter of all SWNTs affected by heat flux in the simulations were fixed. Additionally, to study the effect of diameter on the thermal conductivity of SWNTs, SWNTs with different diameters were examined. However, the length remains the same, 5 nm. Table 3 shows the geometric parameters of SWNTs with smaller and larger diameters. The

largest diameter is approximately 1.65 nm, which results in the sample being triple larger than the one with the smallest diameter [25,27,51,54].

Table 3. Geometric parameters of four groups of SWNTs with different diameters, each group consisting of eight SWNTs with L = 5 nm.

SWNTs (D~0.5 nm)								
Chirality	(6, 0)	(6, 1)	(6, 2)	(5, 2)	(4, 2)	(5, 3)	(4, 3)	(4, 4)
Chiral Angle (°)	0	7.5	13.89	16.1	19.1	21.7	25.28	30
Diameter (nm)	0.48	0.51	0.53	0.5	0.51	0.48	0.45	0.53
SWNTs (D~0.75 nm)								
Chirality	(10, 0)	(10, 1)	(8, 2)	(9, 3)	(8, 4)	(7, 4)	(6, 4)	(6, 6)
Chiral Angle (°)	0	4.7	10.98	13.89	19.1	21.1	23.4	30
Diameter (nm)	0.78	0.79	0.72	0.8	0.79	0.75	0.7	0.78
SWNTs (D~0.95 nm)								
Chirality	(12, 0)	(12, 1)	(11, 2)	(10, 3)	(9, 5)	(8, 5)	(8, 6)	(7, 7)
Chiral Angle (°)	0	3.9	8.2	12.7	20.6	22.4	25.2	30
Diameter (nm)	0.94	0.9	0.94	0.93	0.97	0.9	0.96	0.96
SWNTs (D~1.65 nm)								
Chirality	(21, 0)	(20, 2)	(18, 5)	(17, 6)	(16, 8)	(15, 9)	(14, 10)	(12, 12)
Chiral Angle (°)	0	4.7	11.9	14.6	19.1	21.8	24.5	30
Diameter (nm)	1.67	1.65	1.62	1.64	1.68	1.67	1.64	1.65

In order to obtain reliable thermal properties of the SWNTs via MD simulation, a convergence study on MD simulation time step was conducted. The model to be studied was based on an SWNT with D = 0.95 nm, chirality (12, 0), and L = 5 nm. As shown in Figure 4, the results indicate that a time step of about 0.5 fs or less can provide reliable (converged) simulation results.

For a set of SWNTs with a diameter D of approximate 0.5 nm, a length of 5 nm, and various chiral angles, the thermal conductivity ranges from 43.5 W/m·K to 55.4 W/m·K, as listed in Table 3 and shown in Figure 5, indicating a maximum difference in thermal conductivity of 11.9 W/m·K. The thermal conductivity of the SWNTs increases as the chiral angle increases in a roughly linear pattern. For a set of SWNTs with a diameter D of approximately 0.75 nm, a length of 5 nm, and various chiral angles, the thermal conductivity ranges from 37.5 W/m·K to 50.8 W/m·K, as listed in Table 3 and shown in Figure 5, indicating a maximum difference in thermal conductivity of 13.3 W/m·K. Furthermore, for two sets of SWNTs with a diameter D of approximate 0.95 nm or D of approximate 1.65 nm, a length of 5 nm, and various chiral angles, the maximum differences in thermal conductivity are 14.3 W/m·K and 15.1 W/m·K, respectively. The thermal conductivity of all these sets of SWNTs increases as the chiral angle increases in a roughly linear pattern [25,27,51].

The results show that the effect of the tube diameter on the thermal conductivity of the SWNTs slightly increases with an increase in the tube diameter according to the maximum differences in the thermal conductivity of each set of the SWNTs. In addition, the results listed in Table 3 and shown in Figure 5 show that the thermal conductivity of SWNTs at 300 K is approximately inversely proportional to the diameter of SWNTs, and SWNTs with larger diameters have a lower thermal conductivity than SWNTs with smaller diameters. The results listed in Table 3 and shown in Figure 5 indicate a linear trend for different diameters.

$$\lambda = A\,\theta + B \tag{7}$$

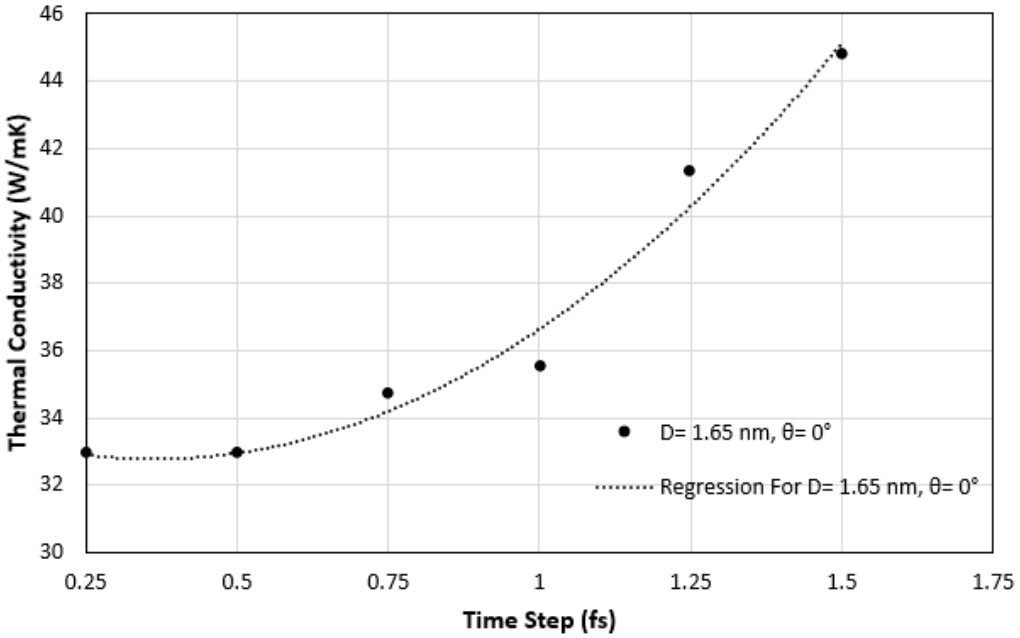

Figure 4. Thermal conductivity convergence study by time step.

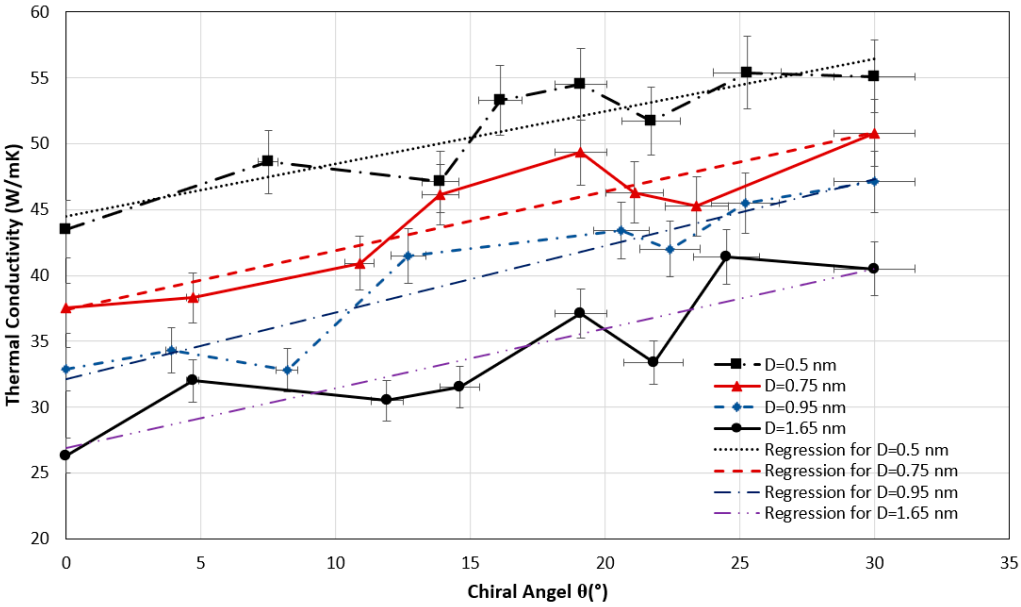

Figure 5. Chiral angle-dependent thermal conductivity of SWNTs with different diameters and a tube length of 5 nm.

The results also show that for D = 1.65 nm, A = 0.45, and B = 26.9 and for other diameters, the quantities of A and B in Equation (7) can be obtained through data linear regression, as listed in Table 4.

Under the same chiral angle, the thermal conductivity of SWNTs changes with the tube diameter, as listed in Table 5 and shown in Figure 6. Under the same chiral angle, the thermal conductivity of SWNTs decreases as the tube diameter increases, and as the tube diameter increases, the thermal conductivity of SWNTs increases greater with larger chiral angles. The thermal conductivity of SWNTs changes with the chiral angle in a power law trend as:

$$\lambda = A\, D^{-B} \tag{8}$$

Table 4. Linear regression results according to the data from Table 3 and Figure 5.

MD Simulation Case	Regression Formula	R^2
SWNTs (D~0.5 nm)	λ = 0.3998 θ + 44.475	0.7954
SWNTs (D~0.75 nm)	λ = 0.4498 θ + 37.396	0.8325
SWNTs (D~0.95 nm)	λ = 0.5062 θ + 32.155	0.8941
SWNTs (D~1.65 nm)	λ = 0.4538 θ + 26.905	0.7777

Table 5. Power law regression results according to the data from Table 3 and Figure 6.

MD Simulation Case	Regression Formula	R^2
SWNTs (θ = 0°)	$y = 32.462x^{-0.428}$	0.9930
SWNTs (θ = 10°)	$y = 36.717x^{-0.382}$	0.9806
SWNTs (θ = 20°)	$y = 42.218x^{-0.338}$	0.9977
SWNTs (θ = 30°)	$y = 46.427x^{-0.262}$	0.9921
SWNTs (θ = 30°) from the literature	$y = 53.068x^{-0.324}$	0.9950

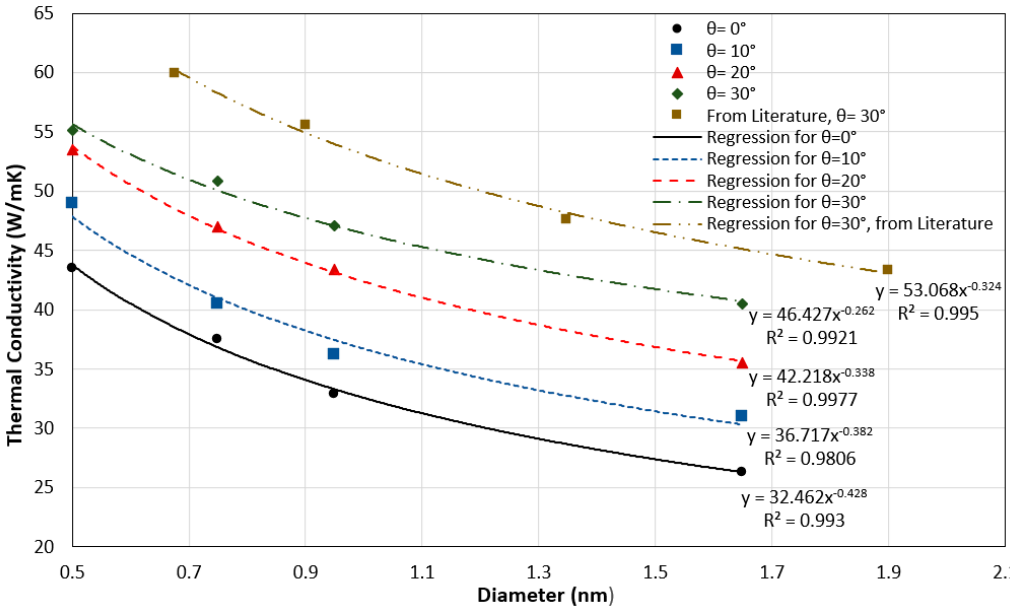

Figure 6. Comparison of the thermal conductivities of single-walled carbon nanotubes with the same chiral angles and different diameters at a fixed length of 5 nm.

The results show that for a chiral angle of 30°, A = 46.48, and B = 0.262, and for other chiral angles, the quantities of A and B are listed in Table 5.

Cao et al. [37] theoretically reported that the thermal conductivity of SWNTs with smaller diameters is higher than that of larger-diameter SWNTs. According to their findings, the thermal conductivity at 300 K decreases with increasing SWNT diameter. Fujii et al. [59] measured the thermal conductivity of SWNTs and found that the thermal conductivity increased as their diameter decreased at room temperature. The thermal conductivity varied from about 500 W/m K for the larger diameter of 28 nm to 2069 W/m K for the smaller diameter of 10 nm. Furthermore, Ya et al. [27] demonstrated that the thermal conductivity of SWNTs with a diameter of approximately 0.95 nm and a length of 20 nm changes by up to 50%, considering different chiral angles. By comparison, the difference for identical SWNTs in diameter was 27% when doubling the diameter of CNTs. In Figure 6, the result of other simulation and experiment findings is shown. Figure 6 shows a comparison

of the data obtained from this study with data from the literature. The thermal conductivity of SWNTs with chirality (5, 5) and (7, 7), D = 0.67 nm, D = 0.9 nm, and L = 5 nm are 59.95 and 55.56 W/m·K, respectively. Also, thermal conductivity for SWNTs with chirality (10, 10) and (14, 14), D = 1.35 nm, D = 1.9 nm, and L = 5 nm are 47.59 and 43.3 W/m·K, respectively [38,57,59].

When the diameter of the CNT is relatively large, the phonons (vibrational energy modes) within the material experience more scattering events, leading to a lower overall thermal conductivity. However, as the diameter of the CNT decreases, the phonons encounter fewer defects or impurities, allowing them to travel more freely. This results in a higher thermal conductivity as the phonons move ballistically along the length of the nanotube without any significant scattering [60].

3.3. Effect of CNT Overlap on Thermal Resistance

Interfacial thermal resistance is the resistance to thermal transport that occurs at the interface between two materials. This resistance arises due to a mismatch in the phonon spectra or vibrational modes between the two materials [61]. The thermal resistance between adjacent CNTs, R, is computed using a triple CNT setup. As shown in Figure 7, the three CNTs belong to the left (CNT_1), right (CNT_2), and middle (CNT_3) parts of the CNT network, respectively, and the symbols h and a denote the vertical normal distance and horizontal overlap, respectively, located between every pair of CNTs. The calculated CNT–CNT interfacial resistance strongly depends on the size of the overlapping CNTs.

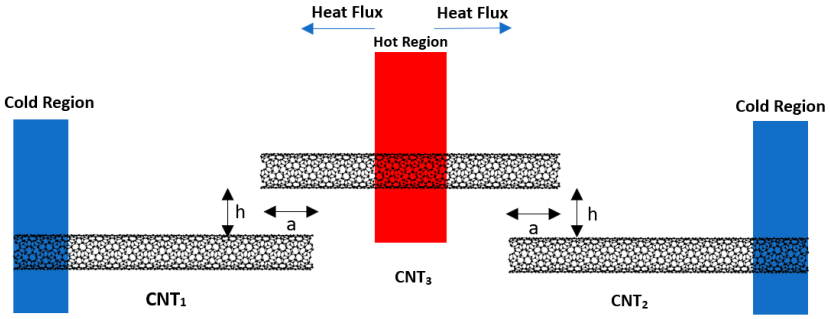

Figure 7. The diagram illustrates a setup comprising three adjacent CNTs used to explore the thermal resistance between the neighboring nanotubes with the overlap of a.

The effect of the overlap length, a, on the thermal resistance, R, is analyzed by adjusting a within the 2–5 nm interval while keeping the tube length, L, constant at 20 nm and the gap between the overlapping CNTs, h, constant at 0.4 nm. The specific selection of h at 0.4 nm is directly related to the equilibrium spacing observed between graphene layers in graphite or within the walls of MWNTs, which is typically 0.342–0.375 nm [61,62]. As shown in Figure 8, R is inversely proportional to the degree of overlap; with the coefficient of determination $R^2 > 0.99$, a power-like trend is observed, that is, $R = C\,a^B$, where $C = 3 \times 10^{-7}$ m^2 K W^{-1}, B = −1.064, and a is expressed in nanometers. Notably, the thermal resistance decreases from 1.4×10^{-8} m^2 K W^{-1} (a = 2 nm) to 5.3×10^{-9} m^2 K W^{-1} (a = 5 nm) due to the enhanced phonon transferring across the broader interfaces. The remarkable decrease in R_{CC} is due to the increased surface available for heat transfer between the contiguous CNTs through van der Waals interactions. Even for different setups, there is a similar decrease in R as the overlap area between CNTs increases. Figure 8 compares the data obtained from this study with data from the literature [63–65]. Zhong and Lukes [63] reported that the interfacial thermal resistance between offset parallel armchair SWNTs decreases as the length of the nanotube increases. Fasano et al. [66] reported that the interlayer thermal resistance is transformed by changing the overlap between SWNTs and the amount of oxygen joints between adjacent SWNTs or DWNTs. They reported that the thermal resistances for SWNTs with L = 10 nm, h = 0.23 nm, and a = 1 and 10 nm are 8×10^{-9} m^2 K W^{-1} and 1.3×10^{-9} m^2 K W^{-1}, respectively. Furthermore,

previous experimental investigations confirmed the derived R values. For example, Yang et al. [67] recorded that the experimental thermal boundary resistance was approximately 1×10^{-9} m^2 K W^{-1} for MWNTs.

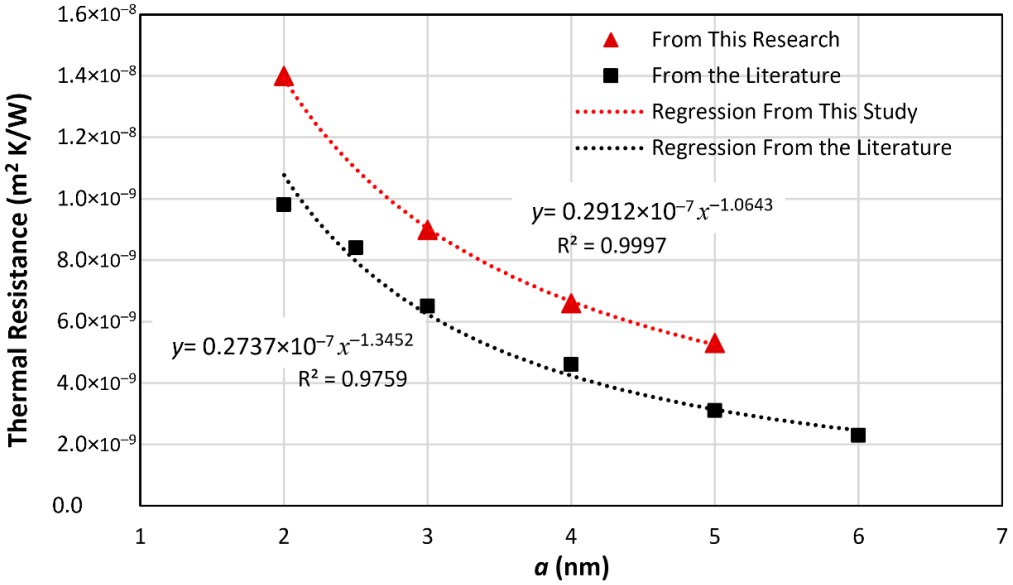

Figure 8. Thermal resistance, R, at the CNT–CNT interface as a function of the horizontal overlap (a), where h is set to 0.4 nm.

4. Conclusions

In the present work, an original computational approach was devised to explore how the atomistic characteristics of CNTs and their interfaces affect the overall thermal conductivity of SWNTs.

The thermal conductivity of SWNTs with different chiralities and lengths were simulated using the RNEMD method to investigate the effect of length on the thermal conductivity of SWNTs. The results show that the thermal conductivity increases as the length increases, and the effect of chirality on the thermal conductivity of SWNTs is more obvious when the tube length is shorter than when the tube length is longer. Furthermore, the results show that when the length of SWNTs is long enough, the thermal conductivity of zigzag SWNTs of the same length is greater than that of armchair SWNTs.

The diameter of SWNTs affects their thermal conductivity. When the tube length becomes longer, the thermal conductivity increases and the effect of chirality on the thermal conductivity decreases; but when the diameter becomes larger, the thermal conductivity does decrease and the effect of chirality on the thermal conductivity increases.

Thermal interfacial resistance between CNTs has been investigated for various nanotube configurations. Increasing tube-to-tube contact dramatically reduces interfacial resistance. Since the interactions between particles rely only on secondary forces (van der Waals forces), heat transfer between adjacent CNTs via van der Waals interactions will increase as the available surface increases.

This study can provide valuable insights into the development of fabrication processes for novel composite materials, which has important implications for contemporary thermal sciences, particularly in the fields of thermal storage and polymeric heat exchangers.

Author Contributions: Conceptualization, L.N.; methodology, L.N.; formal analysis, L.N.; investigation, L.N. and Z.H.; resources, L.N.; data curation, L.N.; writing—original draft preparation, L.N.; writing—review and editing, Z.H.; visualization, L.N. and Z.H.; supervision, Z.H. All authors have read and agreed to the published version of the manuscript.

Funding: This research received no external funding.

Data Availability Statement: Data are contained within the article.

Acknowledgments: This work was supported by the J. J. Lohr College of Engineering and the Mechanical Engineering Department at South Dakota State University, which are gratefully acknowledged.

Conflicts of Interest: The authors declare no conflicts of interest. The funders had no role in the design of the study; in the collection, analyses, or interpretation of data; in the writing of the manuscript; or in the decision to publish the results.

References

1. Bazli, L.; Siavashi, M.; Shiravi, A. A review of carbon nanotube/TiO_2 composite prepared via sol-gel method. *J. Compos. Compd.* **2019**, *1*, 1–9. [CrossRef]
2. Najmi, L.; Zebarjad, S.M.; Janghorban, K. Effects of Carbon Nanotubes on the Compressive and Flexural Strength and Microscopic Structure of Epoxy Honeycomb Sandwich Panels. *Polym. Sci. Ser. B* **2023**, *65*, 220–229. [CrossRef]
3. Saadi, S.; Nazari, B. Recent developments and applications of nanocomposites in solar cells: A review. *J. Compos. Compd.* **2019**, *1*, 41–50. [CrossRef]
4. Pierson, H.O. *Handbook of Carbon, Graphite, Diamonds and Fullerenes*; William Andrew: Albuquerque, NM, USA, 1994.
5. Koumoulos, E.P.; Jagdale, P.; Kartsonakis, I.A.; Giorcelli, M.; Tagliaferro, A.; Charitidis, C.A. Carbon nanotube/polymer nanocomposites: A study on mechanical integrity through nanoindentation. *Polym. Compos.* **2014**, *36*, 1432–1446. [CrossRef]
6. Izadifar, M.A.; Luo, N.; Abu-Farsakh, M.Y.; Chen, S. Performance Evaluation of Design Methods for Geosynthetic-Reinforced Pile-Supported Embankments. *Transp. Res. Rec.* **2023**, *2677*, 458–475. [CrossRef]
7. Bhyrav, M. Thermal Conductivity Characterization of Composite Materials. Ph.D. Thesis, West Virginia University, Morgantown, VA, USA, 2006.
8. Abdolmaleki, M.; Moini Jazani, O.; Moradi, H.; Malayeri, M.; Mehradnia, F. Novel polyethylene glycol/nanosilica Reinforced Polyurethane mixed matrix nanocomposite membrane with enhanced gas separation properties. *Braz. J. Chem. Eng.* **2023**, 1–15. [CrossRef]
9. Mousavi-Bafrouyi, S.S.; Reza, E.F.; Geranmayeh, A. Effect of stacking sequence on the mechanical properties of pseudo-ductile thin-ply unidirectional carbon-basalt fibers/epoxy composites. *J. Ind. Text.* **2022**, *51*, 2835S–2852S. [CrossRef]
10. Alisani, R.; Rakhshani, N.; Abolhallaj, M.; Motevalli, F.; Ghaderi-shekhi Abadi, P.; Akrami, M.; Shahrousvand, M.; Sharifian Jazi, F. Adsorption, and controlled release of doxorubicin from cellulose acetate/polyurethane/multi-walled carbon nanotubes composite nanofibers. *Nanotechnology* **2022**, *33*, 155102. [CrossRef]
11. Woo Lee, S.; Kim, B.S.; Chen, S.; Shao-Horn, Y.; Hammond, P.T. Layer-by-Layer Assembly of All Carbon Nanotube Ultrathin Films for Electrochemical Applications. *J. Am. Chem. Soc.* **2009**, *131*, 671–679. [CrossRef]
12. Ferdosi, S.B.; Porbashiri, M. Calculation of the Single-Walled Carbon Nanotubes' Elastic Modulus by Using the Asymptotic Homogenization Method. *Int. J. Sci. Eng. Appl.* **2022**, *11*, 254–265. [CrossRef]
13. Tajzad, I.; Ghasali, E. Production methods of CNT-reinforced Al matrix composites: A review. *J. Compos. Compd.* **2020**, *2*, 1–9.
14. Alsharef, J.M.A.; Taha, M.R.; Ahmed Khan, T. Physical dispersion of nanocarbons in composites: A review. *J. Teknol.* **2017**, *79*, 7646. [CrossRef]
15. Safavigerdini, K.; Nouduri, K.; Surya, R.; Reinhard, A.; Quinlan, Z.; Bunyak, F.; Maschmann, M.R.; Palaniappan, K. Predicting Mechanical Properties of Carbon Nanotube (CNT) Images Using Multi-Layer Synthetic Finite Element Model Simulations. In Proceedings of the IEEE International Conference on Image Processing (ICIP), Kuala Lumpur, Malaysia, 8–11 October 2023; pp. 3264–3268.
16. Ferdosi Heragh, M.; Eskandarinezhad, S.; Dehghan, A. Ni-Cu matrix composite reinforced with CNTs: Preparation, characterization, wear and corrosion behavior, inhibitory effects. *J. Compos. Compd.* **2020**, *2*, 123–128. [CrossRef]
17. Berber, S.; Kwon, Y.K.; Tománek, D. Unusually High Thermal Conductivity of Carbon Nanotubes. *Phys. Rev. Lett.* **2000**, *84*, 4613. [CrossRef] [PubMed]
18. Najmi, L.; Zhong, H. Effects of Carbon Nanotubes on Thermal Behavior of Epoxy Resin Composites. *J. Compos. Sci.* **2023**, *7*, 313. [CrossRef]
19. Che, J.; Çağin, T.; Goddard, W.A., III. Thermal conductivity of carbon nanotubes. *Nanotechnology* **2000**, *11*, 65–69. [CrossRef]
20. Park, J.; Bifano, M.F.P.; Prakash, V. Sensitivity of thermal conductivity of carbon nanotubes to defect concentrations and heat-treatment. *J. Appl. Phys.* **2013**, *113*, 034312. [CrossRef]
21. Chien, S.-K.; Yang, Y.-T.; Chen, C.-K. The effects of vacancy defects and nitrogen doping on the thermal conductivity of armchair (10, 10) single-wall carbon nanotubes. *Solid State Commun.* **2011**, *151*, 1004–1008. [CrossRef]
22. Faraji, S.; Stano, K.L.; Yildiz, O.; Li, A.; Zhu, Y.; Bradford, P.D. Ultralight anisotropic foams from layered aligned carbon nanotube sheets. *Nanoscale* **2015**, *7*, 17038–17047. [CrossRef]
23. Lee, E.; Salgado, R.A.; Lee, B.; Sumant, A.V.; Rajh, T.; Johnson, C.; Balandin, A.A.; Shevchenko, E.V. Design of lithium cobalt oxide electrodes with high thermal conductivity and electrochemical performance using carbon nanotubes and diamond particles. *Carbon* **2018**, *129*, 702–710. [CrossRef]
24. Alaghemandi, M.; Algaer, E.; Bohm, M.C.; Muller-Plathe, F. The thermal conductivity and thermal rectification of carbon nanotubes studied using reverse nonequilibrium molecular dynamics simulation. *Nanotechnology* **2009**, *20*, 115704. [CrossRef] [PubMed]

25. Qiu, B.; Wang, Y.; Zhao, Q.; Ruan, X. The effects of diameter and chirality on the thermal transport in free-standing and supported carbon-nanotubes. *Appl. Phys. Lett.* **2012**, *100*, 233105. [CrossRef]
26. Charoenpakdee, J.; Suntijitrungruang, O.; Boonchui, S. Chirality effects on an electron transport in single-walled carbon nanotube. *Sci. Rep.* **2020**, *10*, 18949. [CrossRef] [PubMed]
27. Feng, Y.; Zhu, J.; Tang, D.-W. Influence of chirality on the thermal conductivity of single-walled carbon nanotubes. *Chin. Phys. B* **2014**, *23*, 083101. [CrossRef]
28. Behseresht, S.; Mehdizadeh, M. Mode I&II SIFs For Semi-elliptical Crack in a Cylinder Wrapped with a Composite Layer. In Proceedings of the 28th Annual International Conference of Iranian Society of Mechanical Engineers-ISME2020, Tehran, Iran, 27–29 May 2020.
29. Clancy, T.C.; Frankland, S.J.V.; Hinkley, J.A.; Gates, T.S. Multiscale modeling of thermal conductivity of polymer/carbon nanocomposites. *Int. J. Therm. Sci.* **2010**, *49*, 1555–1560. [CrossRef]
30. Silva Hernandez, C.A. Molecular Dynamic Simulation of Thermo-Mechanical Properties of Ultra-Thin Poly (Methyl Meth-acrylate) Films. Ph.D. Thesis, Texas A&M University, Brazos County, TX, USA, 2010.
31. Beitollahpoor, M.; Farzam, M.; Pesika, N.S. Friction force-based measurements for simultaneous determination of the wetting properties and stability of superhydrophobic surfaces. *J. Colloid Interface Sci.* **2023**, *648*, 161–168. [CrossRef]
32. Tajalli, P.; Hernandez Rivera, J.M.; Omidiyan, M.; Tran, H.V.; Lee, T.R. Carbonate-Terminated Self-Assembled Monolayers for Mimicking Nanoscale Polycarbonate Surfaces. *ACS Appl. Nano Mater.* **2023**, *6*, 2472–2477. [CrossRef]
33. Peter, A.; Julio, P. *Physical Chemistry for the Life Sciences*; W. H. Freeman Company: New York, NY, USA, 2006; pp. 469–472.
34. Saito, Y.; Sasaki, N.; Moriya, H.; Kagatsume, A.; Noro, S. Parameter optimization of Tersoff interatomic potentials using a genetic algorithm. *JSME Int. J. Ser. A* **2001**, *44*, 207–213. [CrossRef]
35. Rajasekaran, G.; Kumar, R.; Parashar, A. Tersoff potential with improved accuracy for simulating graphene in molecular dynamics environment. *Mater. Res. Express* **2016**, *3*, 035011. [CrossRef]
36. Osman, M.A.; Srivastava, D. Temperature dependence of the thermal conductivity of single-wall carbon nanotubes. *Nanotechnology* **2001**, *12*, 21. [CrossRef]
37. Cao, J.; Yan, X.; Xiao, Y.; Ding, J. Thermal conductivity of zigzag single-walled carbon nanotubes: Role of the umklapp process. *Phys. Rev. B* **2004**, *69*, 428–433. [CrossRef]
38. Varshney, V.; Lee, J.H.; Brown, J.S.; Farmer, B.L.; Voevodin, A.A.; Roy, A.K. Effect of Length, Diameter, Chirality, Deformation, and Strain on Contact Thermal Conductance between Single-Wall Carbon Nanotubes. *Front. Mater.* **2018**, *5*, 17. [CrossRef]
39. Hou, Q.-W.; Cao, B.-Y.; Guo, Z.-Y. Thermal conductivity of carbon nanotube: From ballistic to diffusive transport. *Acta Phys. Sin.* **2009**, *58*, 7809–7814.
40. Li, W.; Feng, Y.-H.; Tang, J.-J.; Zhang, X.-X. Thermal conductivity and thermal rectification of carbon nanotube Y junctions. *Acta Phys. Sin.* **2013**, *62*, 076107. [CrossRef]
41. Zhang, W.; Zhu, Z.; Wang, F.; Wang, T.; Sun, L.; Wang, Z. Chirality dependence of the thermal conductivity of carbon nanotubes. *Nanotechnology* **2004**, *15*, 936. [CrossRef]
42. Hone, J.; Whitney, M.; Piskoti, C.; Zettl, A. Thermal conductivity of single-walled carbon nanotubes. *Phys. Rev. B* **1999**, *59*, R2514. [CrossRef]
43. Lukes, J.R.; Zhong, H. Thermal conductivity of individual single-wall carbon nanotubes. *ASME J. Heat Mass Transf.* **2007**, *129*, 705–716. [CrossRef]
44. Cahill, D.G.; Ford, W.K.; Goodson, K.E.; Mahan, G.D.; Majumdar, A.; Maris, H.J.; Merlin, R.; Phillpot, S.R. Nanoscale thermal transport. *J. Appl. Phys.* **2003**, *93*, 793–818. [CrossRef]
45. Tascini, A.S.; Armstrong, J.; Chiavazzo, E.; Fasano, M.; Asinari, P.; Bresme, F. Thermal transport across nanoparticle–fluid interfaces: The interplay of interfacial curvature and nanoparticle–fluid interactions. *Phys. Chem. Chem. Phys.* **2016**, *19*, 3244–3253. [CrossRef]
46. Kim, S.Y.; Jang, H.G.; Yang, C.M.; Yang, B. Multiscale prediction of thermal conductivity for nanocomposites containing crumpled carbon nanofillers with interfacial characteristics. *Compos. Sci. Technol.* **2018**, *155*, 169–176. [CrossRef]
47. Müller Plathe, F. A simple nonequilibrium molecular dynamics method for calculating the thermal conductivity. *J. Chem. Phys.* **1997**, *106*, 6082–6085. [CrossRef]
48. Chang, C.W.; Okawa, D.; Garcia, H.; Majumdar, A.; Zettl, A. Breakdown of Fourier's Law in Nanotube Thermal Conductors. *Phys. Rev. Lett.* **2008**, *101*, 075903. [CrossRef] [PubMed]
49. Bui, K. Computational methodologies for estimating thermal boundary resistance and effective thermal conductivity of nanocomposites. In *Thermal Behavior and Applications of Carbon-Based Nanomaterials*; Elsevier: Amsterdam, The Netherlands, 2020; pp. 55–180. [CrossRef]
50. Salaway, R.N.; Zhigilei, L.V. Molecular dynamics simulations of thermal conductivity of carbon nanotubes: Resolving the effects of computational parameters. *Int. J. Heat Mass Transf.* **2014**, *70*, 954–964. [CrossRef]
51. Kumanek, B.; Janas, D. Thermal conductivity of carbon nanotube networks: A review. *J. Mater. Sci.* **2019**, *54*, 7397–7427. [CrossRef]
52. Tersoff, J. New empirical approach for the structure and energy of covalent systems. *Phys. Rev. B* **1988**, *37*, 6991. [CrossRef] [PubMed]
53. Powell, D. Elasticity, Lattice Dynamics and Parameterisation Techniques for the Tersoff Potential Applied to Elemental and Type III-V Semiconductors. Ph.D. Thesis, The University of Sheffield, Sheffield, UK, 2006.

54. Najmi, L.; Zhong, H. Review on Molecular Dynamics Simulations of Effects of Carbon Nanotubes (CNTs) on Electrical and Thermal Conductivities of CNT-Modified Polymeric Composites. *J. Compos. Sci.* **2023**, *7*, 165. [CrossRef]
55. Hana, Z.; Fina, A. Thermal conductivity of carbon nanotubes and their polymer nanocomposites: A review. *Prog. Polym. Sci.* **2011**, *36*, 914–944. [CrossRef]
56. Moreland, J.F. The disparate thermal conductivity of carbon nanotubes and diamond nanowires studied by atomistic simulation. *Microscale Thermophys. Eng.* **2004**, *8*, 61–69. [CrossRef]
57. Maruyama, S. A molecular dynamics simulation of heat conduction in finite length SWNTs. *Phys. B Condens. Matter* **2002**, *323*, 193–195. [CrossRef]
58. Wang, J.; Wang, J.S. Carbon nanotube thermal transport: Ballistic to diffusive. *Appl. Phys. Lett.* **2006**, *88*, 111909. [CrossRef]
59. Fujii, M.; Zhang, X.; Xie, H.; Ago, H.; Takahashi, K.; Ikuta, T.; Abe, H.; Shimizu, T. Measuring the Thermal Conductivity of a Single Carbon Nanotube. *Phys. Rev. Lett.* **2005**, *95*, 065502. [CrossRef] [PubMed]
60. Huang, H.; Huang, X.; Meng, X.; Cheng, Z. Study on interfacial thermal resistance between single wall carbon nanotubes and nickel by molecular dynamics. *J. Phys. Conf. Ser.* **2022**, *2390*, 012070. [CrossRef]
61. Chen, X.; Tian, F.; Clas, P.; Duan, W.; Chen, N.X. Interlayer interactions in graphites. *Sci. Rep.* **2013**, *3*, 3046. [CrossRef] [PubMed]
62. Kiang, C.H.; Endo, M.; Ajayan, P.M.; Dresselhaus, G.; Dresselhaus, M.S. Size Effects in Carbon Nanotubes. *Phys. Rev. Lett.* **1998**, *81*, 1869–1872. [CrossRef]
63. Zhong, H.; Lukes, J.R. Interfacial thermal resistance between carbon nanotubes: Molecular dynamics simulations and analytical thermal modeling. *Phys. Rev. B* **2006**, *74*, 125403. [CrossRef]
64. Bui, K.; Grady, B.P.; Papavassiliou, D.V. Heat transfer in high volume fraction CNT nanocomposites: Effects of inter-nanotube thermal resistance. *Chem. Phys. Lett.* **2011**, *508*, 248–251. [CrossRef]
65. Lee, Y.T.; Shanmugan, S.; Mutharasu, D. Thermal resistance of CNTs-based thermal interface material for high power solid state device packages. *Appl. Phys. A.* **2014**, *114*, 1145–1152. [CrossRef]
66. Fasano, M.; Bozorg Bigdeli, M.; Vaziri Sereshk, M.R.; Chiavazzo, E.; Asinari, P. Thermal transmittance of carbon nanotube networks: Guidelines for novel thermal storage systems and polymeric material of thermal interest. *Renew. Sustain. Energy Rev.* **2015**, *41*, 1028–1036. [CrossRef]
67. Yang, J.; Waltermire, S.; Chen, Y.; Zinn, A.A.; Xu, T.T.; Li, D. Contact Thermal Resistance Between Individual Multi-Wall Carbon Nanotubes. *Appl. Phys. Lett.* **2010**, *96*, 023109. [CrossRef]